Research Article

Daniel Pedraza, Jaime Díez, Isabel-Izquierdo-Barba, Montserrat Colilla, and María Vallet-Regí*

Amine-Functionalized Mesoporous Silica Nanoparticles: A New Nanoantibiotic for Bone Infection Treatment

https://doi.org/10.1515/bglass-2017-0011
Received Oct 27, 2017; revised Dec 04, 2017; accepted Dec 16, 2017

Abstract: This manuscript reports an effective new alternative for the management of bone infection by the development of an antibiotic nanocarrier able to penetrate bacterial biofilm, thus enhancing antimicrobial effectiveness. This nanosystem, also denoted as "nanoantibiotic", consists in mesoporous silica nanoparticles (MSNs) loaded with an antimicrobial agent (levofloxacin, LEVO) and externally functionalized with N-(2-aminoethyl)-3-aminopropyltrimethoxysilane (DAMO) as targeting agent. This amine functionalization provides MSNs of positive charges, which improves the affinity towards the negatively charged bacteria wall and biofilm. Physical and chemical properties of the nanoantibiotic were studied using different characterization techniques, including X-ray diffraction (XRD), transmission electron microscopy (TEM), N_2 adsorption porosimetry, elemental chemical analysis, dynamic light scattering (DLS), zeta (ζ)-potential and solid-state nuclear magnetic resonance (NMR). "In vial" LEVO release profiles and the *in vitro* antimicrobial effectiveness of the different released doses were investigated. The efficacy of the nanoantibiotic against a *S. aureus* biofilm was also determined, showing the practically total destruction of the biofilm due to the high penetration ability of the developed nanosystem. These findings open up promising expectations in the field of bone infection treatment.

Keywords: Mesoporous Silica Nanoparticles; Amine-functionalization; Bacteria and Biofilm targeting; Antimicrobial release; Bone infection treatment

1 Introduction

Bone infection is a potentially dangerous affection that keeps defying the scientific community due to its status as a clinical pathology with important involvements in the socioeconomic field [1–3]. The main trigger agent of this issue is the *Staphylococcus aureus* (*S. aureus*) pathogen [4, 5], and according to databases of PubMed and Scopus, the annual incidence of invasive infections of *S. aureus* varies from 1.6 to 29.7 cases of each 100,000, depending on the studied location. Actually, they come to be the 2.8 from 43% of total infection in bone and joint [6].

Bone infection remains a substantial challenge because of the shortcomings found in current therapies, which relies on the systemic administration of antibiotics and surgery. They are commonly associated to high rate of side effects in the patients, long hospital stays and high morbidity [7].

The development of new strategies that permit to optimize the antimicrobials concentration in the infection site without increasing toxicity would represent a significant advance in the management us such infections. In this context, the entering of nanomedicine into this scenario has revolutionized the scientific research and it is expected that in the forthcoming decades transforms the pharmaceutical and biotechnological industries. The reason underlying this revolution relies on the possibility of circumventing the main limitations of conventional medicine, such as the lack of specificity, narrow therapeutic window,

***Corresponding Author: María Vallet-Regí:** Departamento de Química Inorgánica y Bioinorgánica, Facultad de Farmacia, Universidad Complutense de Madrid, Instituto de Investigación Sanitaria Hospital 12 de Octubre i+12, Plaza Ramón y Cajal s/n, 28040 Madrid, Spain; CIBER de Bioingeniería, Biomateriales y Nanomedicina, CIBER-BBN, Madrid, Spain; Email: Email: vallet@ucm.es; Tel.: +34 91 394 18 61; Fax: +34 91 394 17 86

Daniel Pedraza, Jaime Díez: Departamento de Química Inorgánica y Bioinorgánica, Facultad de Farmacia, Universidad Complutense de Madrid, Instituto de Investigación Sanitaria Hospital 12 de Octubre i+12, Plaza Ramón y Cajal s/n, 28040 Madrid, Spain

Isabel-Izquierdo-Barba, Montserrat Colilla: Departamento de Química Inorgánica y Bioinorgánica, Facultad de Farmacia, Universidad Complutense de Madrid, Instituto de Investigación Sanitaria Hospital 12 de Octubre i+12, Plaza Ramón y Cajal s/n, 28040 Madrid, Spain; CIBER de Bioingeniería, Biomateriales y Nanomedicina, CIBER-BBN, Madrid, Spain

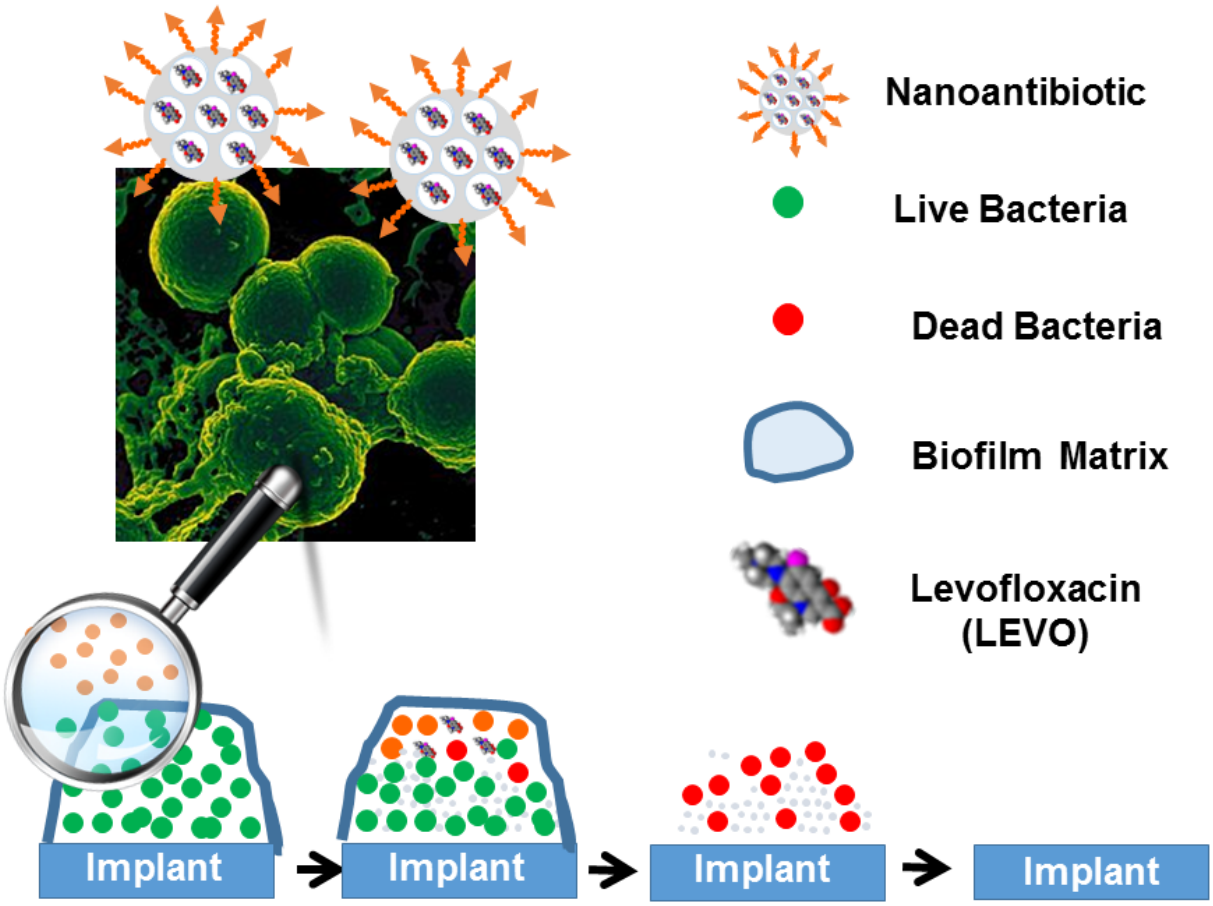

Figure 1: Representative depiction of the mechanism of action of the nanoantibiotic against bacterial biofilm.

low solubility and stability, unappropriated pharmacokinetics and diverse side effects of drugs [8]. Albeit during the last 40 years promising results have been achieved, the clinical application of nanotechnology, in its broadest sense, remains an enormous defy. This fact can be explained because nanomedicine requires complex and specific technological solutions that make difficult its pharmaceutical development [9]. The application of nanomaterials in medicine has provided more than 250 products already approved or in different phases of clinical trials.

Nowadays, one of the most important challenges in bone infection therapy is the design of nanocarriers able to protect, transport and release antimicrobial agents in a controlled way once they reached the target (bacteria and biofilm) [8, 10]. Among nanocarriers, mesoporous silica nanoparticles (MSNs) are excellent candidates to develop targeted stimuli-responsive drug delivery systems [9, 11–19]. They exhibit unique properties such as high specific surface area, large pore volume, tunable pore structures and easily modifiable surface due to the presence of silanol groups (Si-OH) [10, 20]. Moreover, MSNs have been demonstrated to be biocompatible both *in vitro* and *in vivo* [21–23] and exhibit adequate stability in different biological media [24, 25].

Herein, we designed a nanosystem named "nanoantibiotic" as a new therapeutic alternative to fight against bone infection. This nanoantibiotic, which is based on MSNs, combines an antimicrobial agent with an amine functionalization as targeting agent to recognize the bacteria. Levofloxacin (LEVO) antibiotic, a wide range fluoroquinolone usually employed in osteomyelitis and implant associated bone infections due to its strong cortical bone affinity [26] was used. The used targeting agent, N-(2-aminoethyl)-3-aminopropyltrimethoxysilane (DAMO), deploys positively charged amine groups on the MSN surface that enables attractive electrostatic interactions with the bacteria wall and/or biofilm, exhibiting negative density charge. The hypothesis of the current research work is schematically depicted in Figure 1.

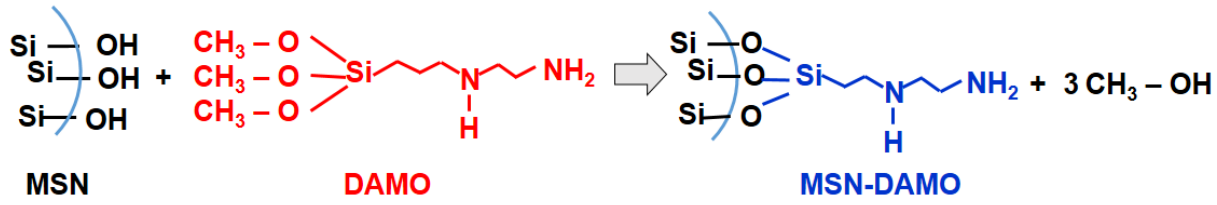

Figure 2: Scheme of the DAMO grafting to the Si-OH present on the MSN external surface.

2 Materials and Methods

2.1 Synthesis and functionalization of MSNs

Pristine MSNs, denoted as MSN, were synthesized *via* the modified Stöber method [27]. Briefly, 1 g of cetyl trimethylammonium bromide (CTAB, Sigma-Aldrich) was dissolved in 480 mL Milli-Q water (resistivity 18.2 MΩ cm) containing 3.5 mL of a 2M solution of NaOH (99%, Sigma-Aldrich). The mixture was kept under magnetic stirring (400-600 rpm) at 80°C for 45 min. Afterwards, 5 mL of tetraethyl orthosilicate (TEOS, 98%, Sigma-Aldrich) were added with a pump injector NE-300 (Just Infusion) at a rate of 0.33 mL/min, maintaining the same conditions of temperature and stirring for 2 h. Later, the flask was cooled down rapidly and its content was centrifuged in a centrifuge Heraeus Multifugue X3 (Thermo Fisher Scientific) at 10,000 rpm and 10°C for 10 min in 3 cycles. Between each cycle, the content was resuspended with 80 mL of absolute ethanol (99.5%, PanReac), for its washing. Finally, the obtained product was dried in a vacuum stove (Vaciotemp-T JP Selecta, ICT) at 30°C. To provide the MSNs fluorescent properties for detecting them using confocal microscopy, this synthesis route was modified by adding fluorescein. For this purpose, 1 mg of fluorescein isothiocyanate (FITC, Sigma-Aldrich) was added to 2.2 µL of (3-aminopropyl)triethoxysilane (APTES, 99%, ABCR) and 100 µL of absolute ethanol under constant stirring at 200 rpm for 2h at room temperature (RT) and protected from light. After this time, 5 mL of TEOS were added until complete homogenization was obtained. This solution was injected in the synthesis flask containing the aqueous solution of the structure-directing agent in basic medium, as indicated for the preparation of the MSN.

To provide MSN of targeting properties towards bacteria, their surface was functionalized with N-(2-aminoethyl)-3-aminopropyltriethoxysilane (DAMO, 95%, ABCR) by means of a post-synthesis grafting under anhydrous conditions and inert atmosphere [28]. The reaction was produced through the condensation between the DAMO molecules and the silanol groups on the MSN surface, as indicated in Figure 2. The functionalization was carried out before the surfactant removal from the mesoporous cavities, in such a way that the material is only functionalized in the exterior, leaving the pores free after the extraction process [29]. The amount of DAMO used for the functionalization process was calculated taking into account the average superficial density of silanol groups in the MSNs (4.9 SiOH/nm^2) [30] and the fact that each DAMO molecule mainly condenses with three Si-OH groups (in good agreement with the results derived from ^{29}Si NMR, *vide infra*). Briefly, 1 g of MSN was dried in a three-mouthed flask with round bottom at 80°C and vacuum conditions for 24 h. Then, three cycles alternating vacuum and N_2 were performed. 200 mL of anhydrous toluene (99.8%, Sigma-Aldrich) were added and the flask was immersed in a ultrasound bath for 1 h. Afterwards, 0.8 mL of DAMO were added and the flask was left at 110°C with reflux for 24 h. Finally, the product was centrifuged by successive washing cycles with isopropanol, ethanol and methanol, respectively. The product was left to dry for 24 h under vacuum at 30°C. The surfactant extraction was performed *via* cationic exchange. For this purpose, an extracting solution containing 100 mL of deionized water, 1.9 L of ethanol and 20 g of NH_4NO_3 (99.5%, Sigma-Aldrich) was made. Then, 1 g of MSNs was added to 600 mL of extracting solution. The suspension was kept during 24 h with a reflux (80°C) and magnetic stirring. Finally, the product was washed 3 times with ethanol and was left to dry for 24 h at 30°C in a vacuum oven.

2.2 Materials Characterization

The structural characterization was performed using X-ray diffraction (XRD) in a diffractometer Philips X'pert Plus working with K_α radiation of Cu (λ = 1.54 Å) at 40 kV and 20 mA, in the range 0.6-7° with a contact time of 5 s and transmission electronic microscopy (TEM) in a JEOL JEM 1400 microscope with a voltage accelerator of 120 kV with a CCD of 2048 x 2048 pixels. The textural properties were determined using porosimetry of N_2 adsorption at –196°C using a Micromeritics ASAP 2020 analyzer (Mi-

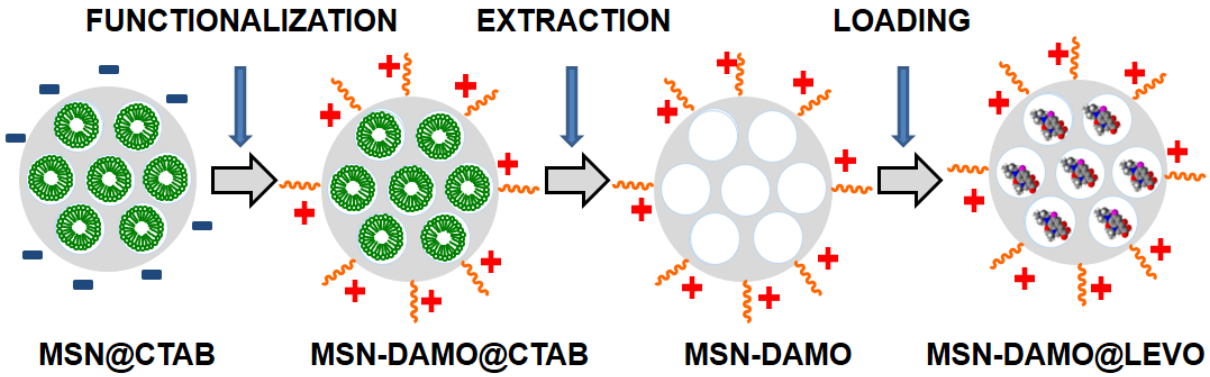

Figure 3: Sequential process of functionalization, extraction and LEVO loading of MSNs affording MSN-DAMO@LEVO.

cromeritics Co.). The surface area was calculated using the Brunauer-Emmet-Tellet (BET) method [31]. The total pore volume (V_T) was estimated from the N_2 adsorbed at a relative pressure of 0.97. The pore diameter (Dp) was determined using the Barret-Joyner-Halenda (BJH) method. The hydrodynamic size was determined via dynamic light scattering (DLS) in a Zetasizer Nano ZS (Malvern Instruments Ltd.) equipped with a 633 nm laser. The same equipment was used to measure the ζ-potential. The chemical composition was determined via elemental chemical analysis in a Perkin-Elmer 2400 CHNS thermoanalyzer. The changes in the chemical environments of the Si and C atoms of the different samples were studied through ^{29}Si (single pulse, SP, and cross-polarization, CP) and $^{1}H \rightarrow {}^{13}C$ solid-state nuclear magnetic resonance (NMR) in a Bruker AV-400-WB spectrometer, using spinning speeds of 10 and 12 kHz and observation frequencies of 79.49 and 100.62 MHz, respectively. The ^{29}Si spectra were obtained using a single pulse sequence (^{29}Si SP magic angle spinning, MAS, NMR), whilst the ^{13}C ones were obtained using a $^{1}H \rightarrow {}^{13}C$ CP MAS NMR sequence. The time periods between successive collections were 5 and 3 ms for ^{29}Si and ^{13}C, respectively, and the total number of scans was approximately 1,000 for both cases.

2.3 Levofloxacin loading and drug release

The loading of LEVO (≥ 98.0%, Sigma-Aldrich) inside the matrix of MSN and MSN-DAMO was done *via* the impregnation method [32]. 125 mg of MSN and MSN-DAMO was suspended in 25 mL of a drug solution (26.1 mg/mL) in the absence of light under magnetic stirring during 24 h at RT, and the resulting samples were denoted as MSN@LEVO and MSN-DAMO@LEVO, respectively. Figure 3 schematically shows the full process followed to obtain MSN-DAMO@LEVO.

The release of LEVO from each of the matrices was done under *in vitro* conditions at 37°C and physiological pH (pH 7.4). A solution of 4 mg of the loaded materials was prepared in 500 µL of phosphate buffered saline (PBS 1x, Sigma Aldrich). 170 µL of this suspension was introduced in a release cap and placed in a bucket containing 3.6 mL of PBS separated by a dialysis membrane that only allows for the diffusion of LEVO molecules. The system was kept at 37°C under magnetic stirring and the concentration of released drug was monitored *via* fluorescence in a Biotek-Powerwave XS with the programme Gen5 (v.1.00.14), using a λ(exc)=292 nm y λ(em)=494 nm. To determine the LEVO concentration a calibration curve in the 12 to 0.02 µg/mL range was performed. The "in vial" release study was carried out by renewing the media at given times. With the aim of determining the effectiveness of the different released LEVO doses against bacteria growth, 100 µL of each dose was inoculated in 900 µL of suspension containing 10^8 bacteria/mL in PBS, which was later incubated overnight at 37°C and under orbital stirring at 200 rpm. This study was performed with Gram-positive (*S. aureus*) and Gram-negative (*E. coli*) bacteria. The presence (or absence) of bacteria, along with its quantification was done by means of counting the colony forming units (CFUs) on tryptic soy agar (TSA, Sigma-Aldrich) plates. For this purpose 10 µL of this solution was seeded in TSA plates, being incubated at 37°C overnight, with a later counting of the CFUs. All the assays were done in triplicate with their respective control samples.

2.4 *In vitro* antimicrobial tests

The nanoantibiotic effectiveness was determined using three different approaches: targeting to the bacteria wall, targeting to bacterial biofilm, and antimicrobial activity against preformed *S. aureus* biofilm.

Targeting to bacteria: In this study Gram-negative bacteria *E. coli* ATCC25922 collection strain was used. Before the assays, disk-shaped cover glasses (9 mm diameter) were sterilized by UV-light and then incubated with poly-D-lysine (0.3 mL per well from a 0.1 mg/mL stock solution in Dulbecco's Phosphate Buffered Saline, Sigma-Aldrich) for 90 min at 37 °C. Then, the excess poly-D-lysine was removed by washing with sterilized Milli-Q water and the cover glasses were left to dry overnight in a sterile environment. Poly-D-Lysine treated cover glasses were placed in 24 well culture plates (CULTEK). Then, 500 µL of the 10^8 bacteria/mL solution was added onto each cover glass and subsequently 500 µL of FMSNs and FMSNs-DAMO suspensions in PBS at different concentrations (5 and 10 μg/mL) were also inoculated and incubated at 37°C and 200 rpm under orbital stirring during 90 min. Then, each glass-disk was washed twice with sterile Hank's balanced salt solution (HBSS, Sigma-Aldrich) and 1mL of HBSS was added. FM 4-64FX dye (0.2 mL from a 5 µg/mL stock solution in HBSS, Invitrogen) was added to stain the bacteria wall in red and incubated on ice for 10 min under orbital stirring. Later on, the cover glasses were washed with HBSS and fixed in 2% wt/vol paraformaldehyde in PBS for 10 min at RT. The fixative was removed with HBSS twice and 0.5 mL HBSS was added to each well before imaging. The samples were examined in an Olympus FV1200 confocal microscope.

Targeting to bacterial biofilm: *S. aureus* ATCC28213 strain was used for these studies. After treating with poly-D-lysine, as above described, the cover glasses were placed in a 24 well culture plate and 500 µL of a solution of bacteria with 10^8 bacteria per mL were added to each plate during 48 h. Then, 500 µL of fluorescent MSN and MSN-DAMO suspensions at different concentrations (10 and 20 µg/mL) in PBS was added and incubated at 37°C under orbital stirring at 200 rpm. The medium used was 66% TSB + 0.2% glucose (wt/vol) to promote robust biofilm formation. After 90 min, the treated cover glasses were washed three times with sterile PBS, stained with 5 µL/mL calcofluor (calcofluor white, Sigma-Aldrich) and incubated during 15 min. The calcofluor stained the mucopolysaccharides of the biofilm (extracellular matrix in blue). The samples were examined in an Olympus FV1200 confocal microscope. Control biofilms without nanoparticles was also observed.

Antimicrobial effects against Gram positive S. aureus biofilm: Effectiveness of the complete nanosystems containing both targeting and antimicrobial LEVO agents against bacterial biofilm was determined. For these purpose, *S. aureus* biofilms were developed, as above described. Then, 0.5 mL of the suspension of nanoparticles in PBS at a concentration 10 µg/mL was added. After 90 min of incubation, the cover glasses were washed three times with sterile PBS, stained with a 3 µL/mL of Live/Dead® Bacterial Viability Kit (Backlight™, Invitrogen) and 5 µL/mL of calcofluor solution was added. Both reactants were incubated during 15 min at RT. Biofilm formation was examined in an Olympus FV1200 confocal microscope. Bacterial biofilm control was also studied. Eight photographs (60x magnification) of each sample were taken. The surface area covered by adhered bacteria was calculated using ImageJ software (National Institute of Health, Bethesda, MD). The experiments were performed in triplicate.

3 Results and discussion

3.1 Sample Characterization

The structural and textural characterization of MSNs before and after DAMO functionalization was performed using TEM, XRD and N_2 adsorption porosimetry (Figure 4).

TEM images show a spherical morphology of nanoparticles sized *ca.* 120 nm, showing a honeycomb disposition of the inner channels that follow a hexagonal symmetry. XRD diagrams confirm that structure, showing diffraction maxima at 2.3°, 3.9° and 4.5° which can be indexed as the 10, 11 and 20 reflections, respectively, of a 2D hexagonal structure *p6mm* plain group. In terms of textural properties, the adsorption-desorption N_2 isotherms profiles are associated to mesoporous MCM-41 type materials with cylindrical parallel pores. Table 1 contains structural parameters (surface area(S_{BET}), pore volume (V_P), pore diameter (D_P)) of samples before and after functionalization, showing a decrease of them after DAMO grafting. Additionally, using the lattice parameter (a_0) obtained by XRD and D_p, we can obtain wall thickness, which increases after the functionalization process. We can observe a reduction on hydrodynamic size (D_H) of MSN-DAMO against MSN due to DAMO's hydrophilic behavior, which provides a higher colloidal stability. The ζ-potential change means a change on the sign of the surface charge density, which confers MSN-DAMO of potential bacterial targeting capability.

Quantitative determination of functional groups, performed by elemental chemical analysis, indicated that the amount of DAMO incorporated into MSN-DAMO was 286 mg/g. With the aim of evaluating the modification in the chemical environments of MSNs we carried out solid state

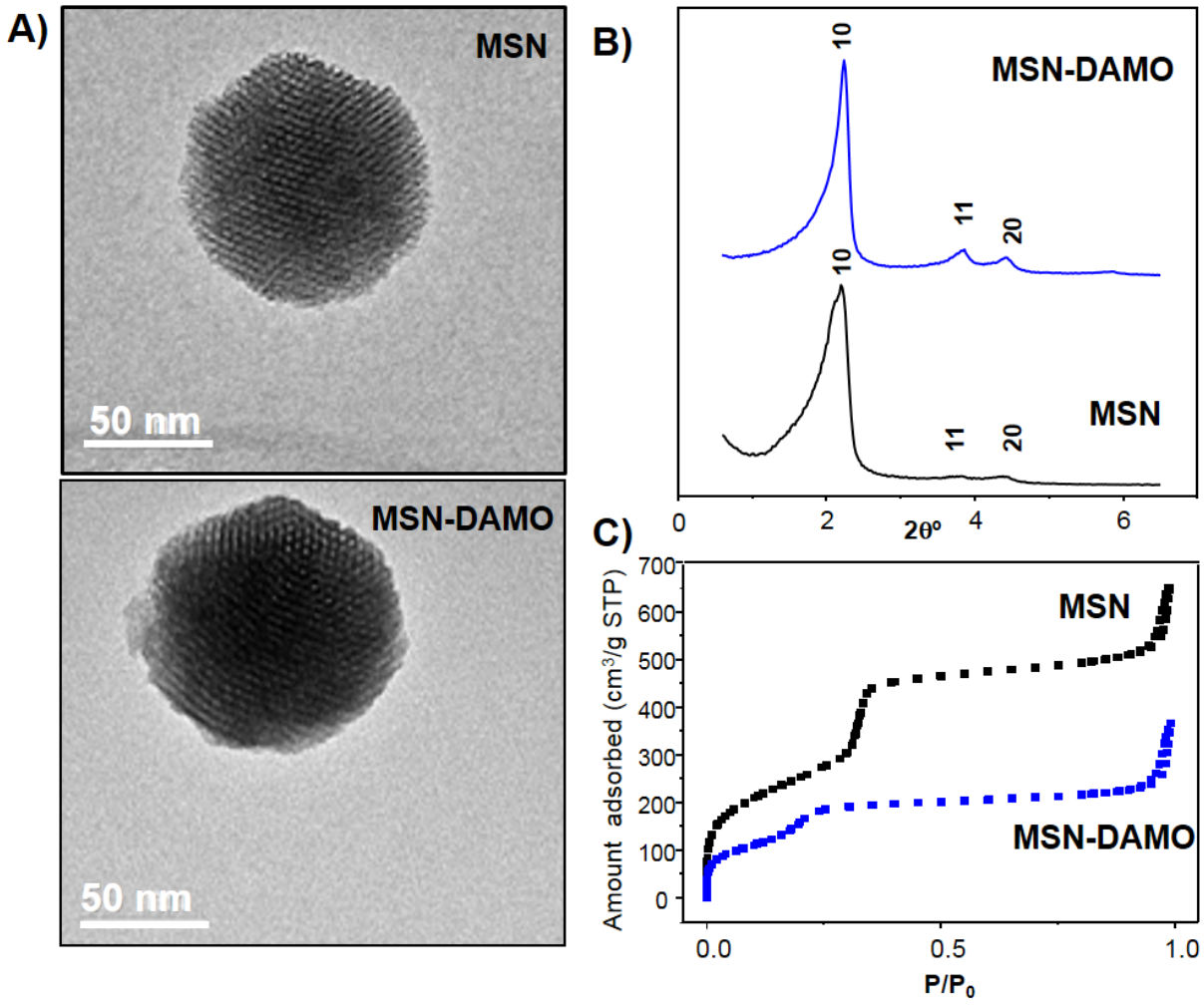

Figure 4: (A) TEM images, (B) XRD patterns and (C) N_2 adsorption isotherms of MSN and MSN-DAMO.

Table 1: Lattice parameter (a_0), hydrodynamic size (D_H), textural properties, ζ-potential and weight (%) of DAMO and LEVO for the different samples.

Sample	a_0 (nm)	D_H(nm)	S_{BET} (m^2/g)	V_P (cm^3/g)	D_P (nm)	t_{wall} (nm)	ζ-pot. (mV)	% DAMO	% LEVO
MSN	4.55	190	937	0.85	2.4	2.1	−36.4	0	0
MSN-DAMO	4.68	141	670	0.40	2.1	2.5	37.4	28.6	0
MSN@LEVO	4.50	183	798	0.73	2.6	1.9	−37.0	0	3.18
MSN-DAMO@LEVO	4.51	139	294	0.25	1.9	2.6	+35.1	28.6	5.03

NMR studies. Figure 5 shows CP-MAS and SP-MAS of ^{29}Si spectra of samples and Table 2 displays the relative abundance of Si species in the different environments derived from the deconvolution and subsequent integration of the resulting peaks. Both MSNs spectra show resonances at −94, −102 y −111 ppm, which are assigned to silicon atoms in Q^2, Q^3 and Q^4 environments. Q^2 and Q^3 structural units are ascribed to the Si-OH groups present on the MSN surface. The relative abundances of Si atoms in Q^2 and Q^3 environments decrease in the case of functionalized sample, due to the condensation reaction of DAMO moieties with the Si-OH groups of MSN surface. Furthermore, MSN-DAMO spectrum shows two additional peaks associated to organosiloxane groups T^2 and T^3 at *ca.* −59 and −68 ppm, respectively. These data confirm the presence of covalent unions between the MSN surface and DAMO molecules.

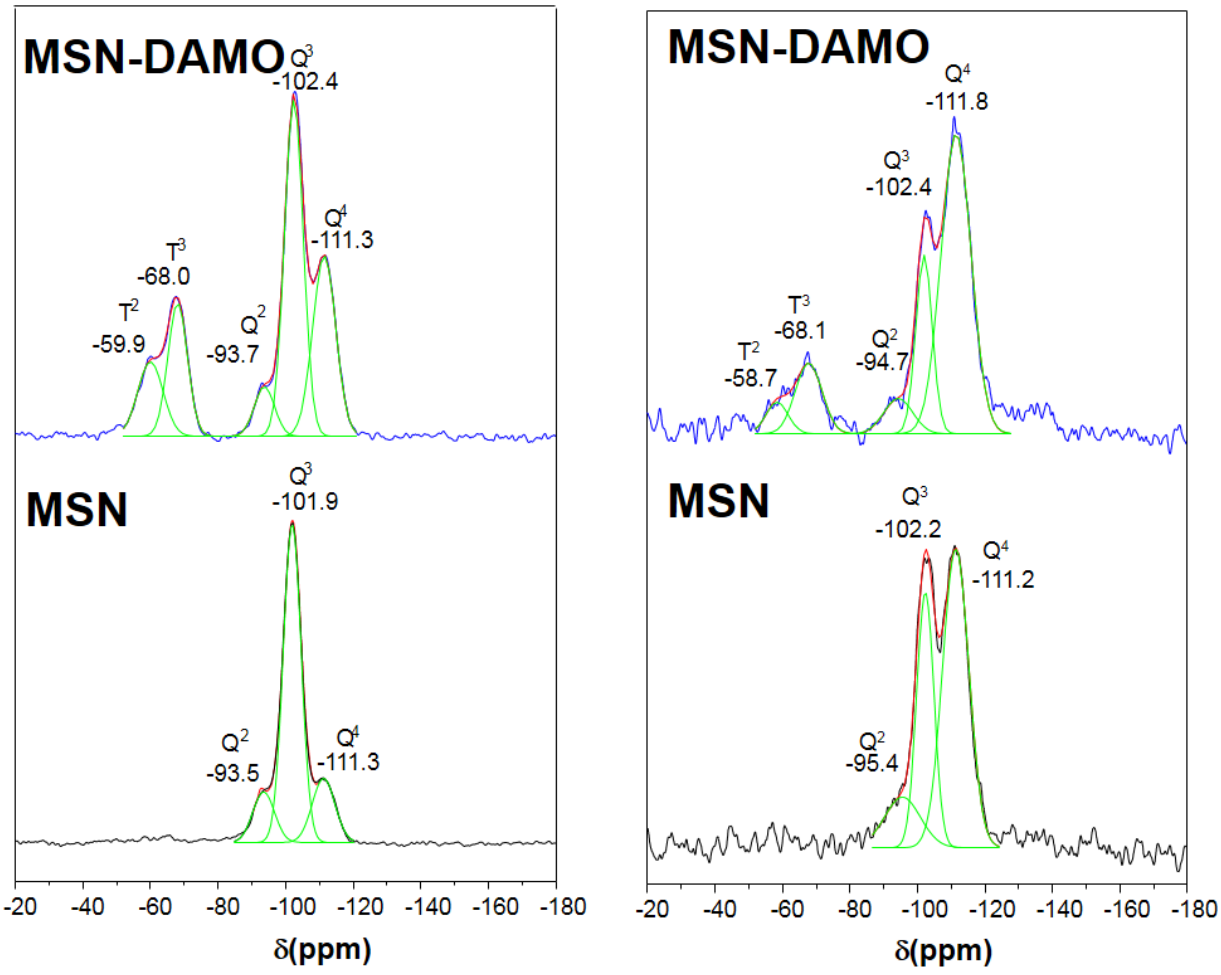

Figure 5: Left) $^{1}H \rightarrow ^{29}Si$-CP-MAS NMR results of MSN and MSN-DAMO that indicate the maxima position of Q^n y T^m. Right) $^{1}H \rightarrow ^{29}Si$-SP-MAS NMR results of MSN and MSN-DAMO.

Table 2: Relative abundance of species of Si on Q^n and T^m environments obtained from the deconvolution of the ^{29}Si SP-MAS NMR signals.

Sample	% T^2	% T^3	% Q^2	% Q^3	% Q^4
MSN	0	0	13	31	56
MSN-DAMO	5	12	6	19	58

In MSN spectrum maxima corresponding to remaining CTAB are observed, while in MSN-DAMO signals associated to various C atoms of DAMO appear, whose assignation is also included in Figure 6.

3.2 Levofloxacin loading and release assays

The amount of LEVO incorporated to samples was determined by elemental chemical analysis, resulting in 31.8 mg/g and 50.3 mg/g for MSN@LEVO and MSN-DAMO@LEVO, respectively. Figure 7 represents the release curves of LEVO from the different matrices. The results show that LEVO release from MSN is slower than from MSN-DAMO, which also produces a partial retention of the drug in the former. On the contrary, drug release profile from MSN-DAMO follows a typical diffusion model, where almost the total loaded LEVO is released after 72 h of assay. Both release curves were analyzed and compared with Chapman equation (Eq. 1) [28, 33]:

$$\frac{w(t)}{w_0} = A\left(1 - e^{-kt}\right)^{\delta} \quad (1)$$

where $w(t)$ is the amount of LEVO released at t time, w_0 is the initial amount of loaded drug, A is the maximum LEVO release, k is the release kinetic constant and δ is a dimensionless parameter of non-ideality that characterizes the release.

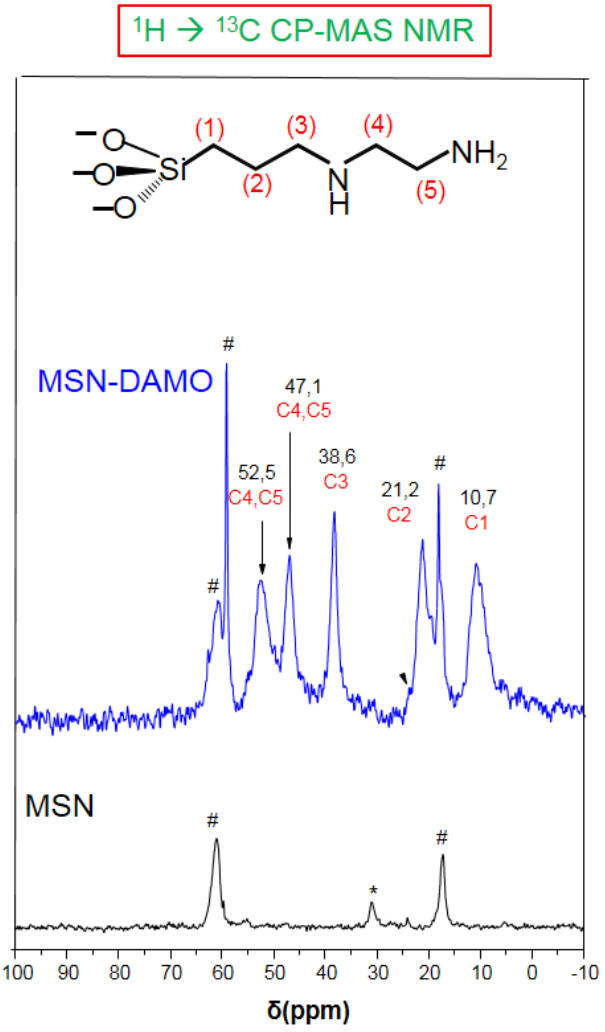

Figure 6: $^{1}H \rightarrow {}^{13}C$ CP-MAS NMR spectra of MSN and MSN-DAMO. On the top, the assignation to different carbon atoms of DAMO is shown.

In both cases, δ is minor than 1, showing that the behavior is different from a first order kinetic. The k values varies from 0.021 to 0.51 h^{-1} for MSN@LEVO and MSN-DAMO@LEVO, respectively, which could point to strong attractive interactions of the LEVO molecules with the Si-OH groups present in the matrix of pristine MSN, as it has been demonstrated elsewhere [34].

The effectiveness of the different released LEVO doses at several times from both MSNs against *E. coli* and *S. aureus* bacterial growth was performed. The counting of CFUs after 1, 3 and 24 h showed the efficacy from both matrices against the two tested strains (data not shown).

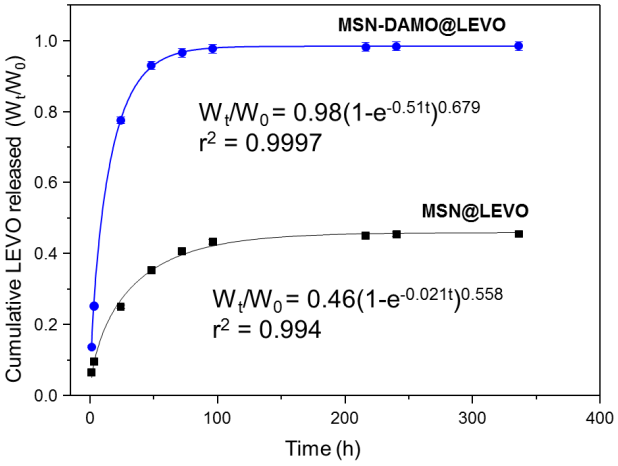

Figure 7: Cumulative LEVO release profiles from MSN and MSN-DAMO samples and comparison with Chapman equation.

3.3 Targeting to bacteria wall and biofilm

Regarding targeting to bacteria wall (Figure 8), confocal images reveal that fluorescent MSN-DAMO are located near the *E. coli* bacteria wall resulting in aggregates of nanoparticles (green dots) on the bacteria's surface for both tested concentration. Note than in the case of MSN such green dots are not observed, probably due to the lack of interaction with the bacteria wall and that would be easily removed during the washing process.

Concerning targeting to bacterial biofilm, Figure 9 represents the effect of DAMO functionalization (MSN-DAMO, green), to *E. coli* biofilm (blue) investigated by using confocal microscopy at different depths. It can be appreciated noticeable differences between MSN and MSN-DAMO. Thus, in the case of MSN, the nanoparticles are localized in the vicinity of the biofilm. However, for MSN-DAMO it can be observed that the nanoparticles are internalized within biofilm, demonstrating the capability of this amine-functionalized nanosystem to penetrate the mucopolysaccharide matrix.

3.4 Nanoantibiotic efficacy

Once demonstrated the ability of MSN-DAMO nanoparticles to target the bacteria wall and internalize into the biofilm, we measured the effectiveness of the complete nanosystem (MSN-DAMO@LEVO) against a previously formed *S. aureus* biofilm. We chose such bacterial strain since it is the most common responsible of bone infection processes [4]. Figure 10 represents the confocal microscopy study corresponding to the preformed *S. aureus* biofilm before and after being treated with MSN@LEVO

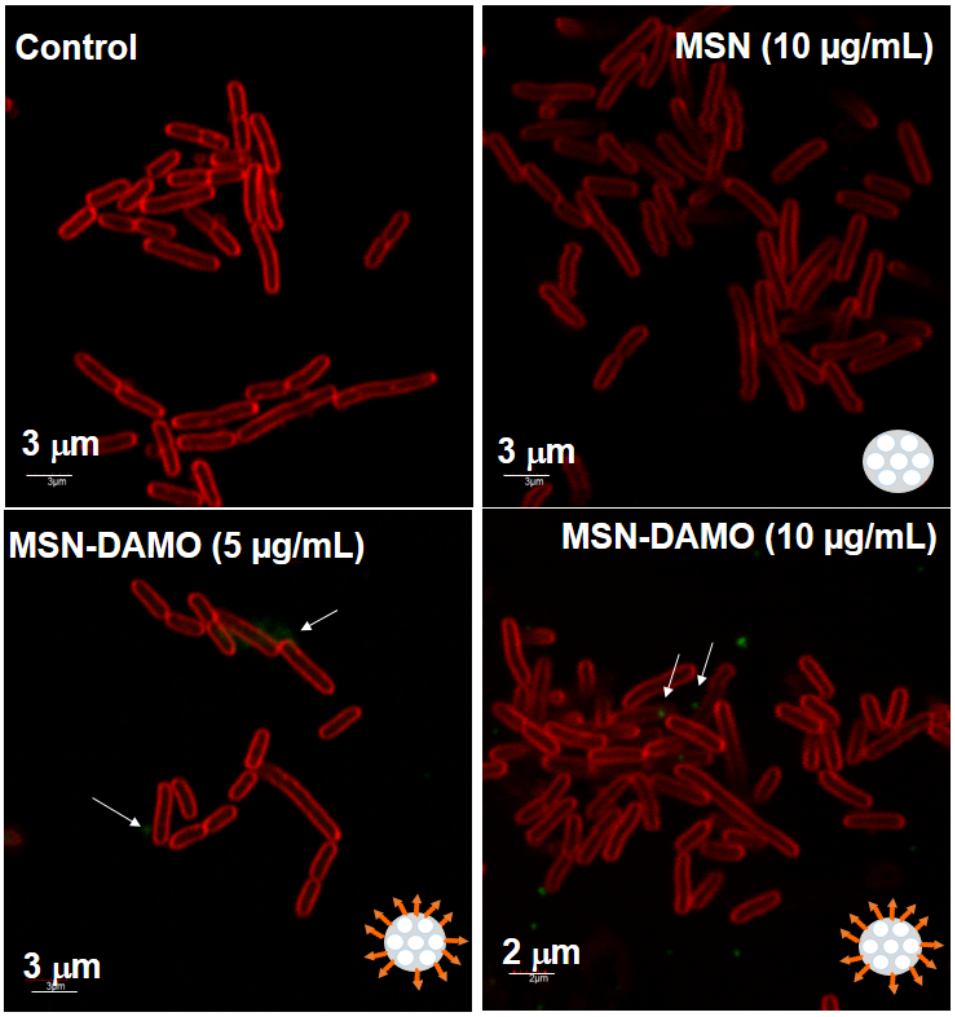

Figure 8: Targeting to *E. coli* bacteria wall studies by confocal microscopy.

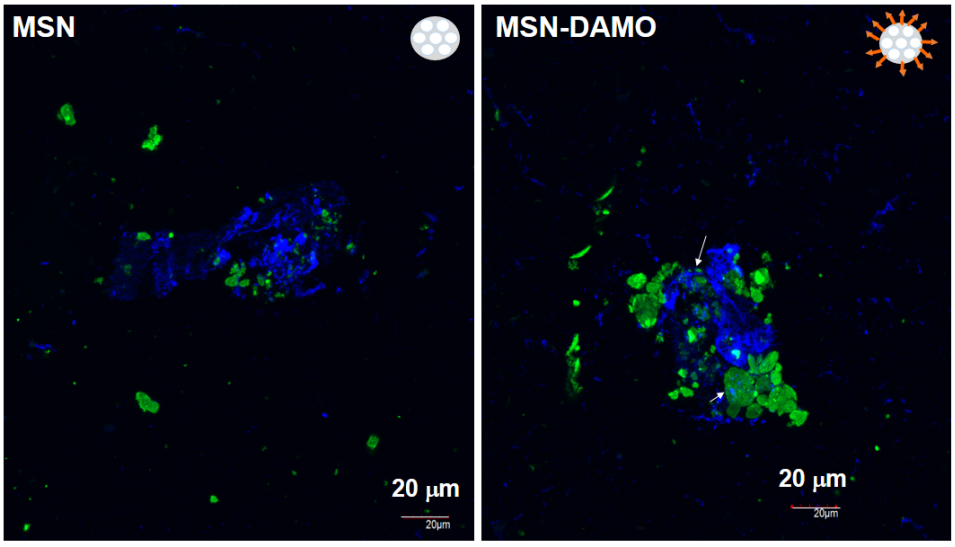

Figure 9: Targeting to *E. coli* biofilm studies by using confocal microscopy.

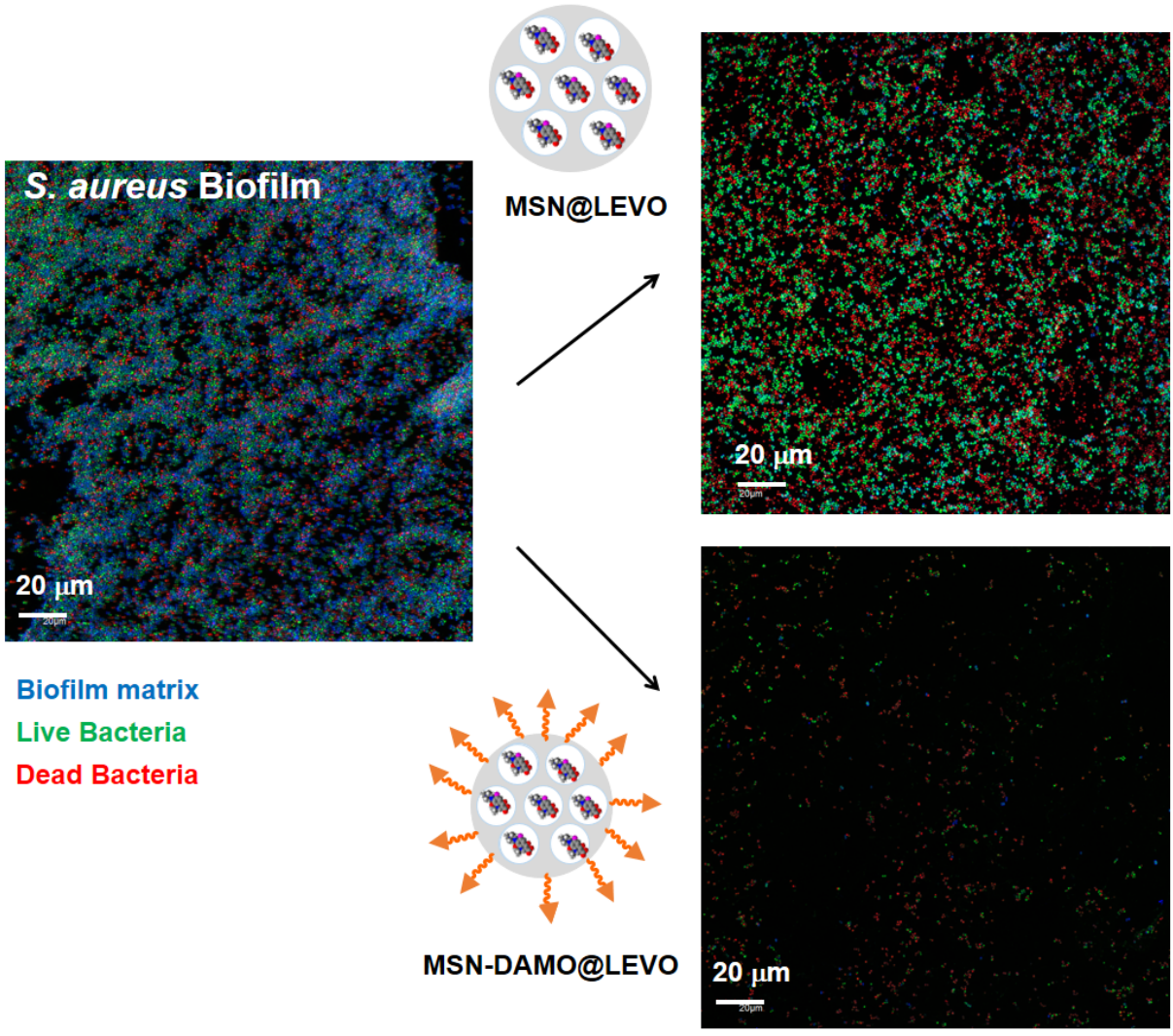

Figure 10: Left: Control biofilm. Right: Biofilm treated with MSN and MSN-DAMO nanosystems.

and MSN-DAMO@LEVO. The results show that the untreated biofilm is composed of live bacteria multilayer (green) with a small amount of dead bacteria (red) coated by a polysaccharide matrix (blue) with an average thickness of 35 µm. After treatment with MSN@LEVO a remaining bacteria layer mainly formed by live cells is observed. Nonetheless, in the case of the full MSN-DAMO@LEVO nanosystem the complete destruction of biofilm is appreciated, appearing only isolated bacteria, almost negligible. These results evidence that the incorporation of a targeting agent onto the MSNs platform triggers the complete biofilm destruction in combination with antibiotics.

4 Conclusions

We have developed a new nanoantibiotic consisting on mesoporous silica nanoparticles decorated with amine groups on their surface and loaded with levofloxacin into their mesopores. Amine-functionalization provides this nanocarrier of a positive charge density that improves the targeting capability of the nanosystem to bacteria wall and bacterial biofilm, meanwhile improving the antibiotic release by achieving faster release kinetics. Microbiological studies against *S. aureus* biofilms show the complete destruction of biofilm when both elements (antibiotic and targeting agents) are synergistically combined in a unique nanoplatform. We envision this nanoantibiotic as a promising alternative to current therapies for the treatment of bone infection.

Acknowledgement: MVR acknowledges funding from the European Research Council (Advanced Grant VERDI; ERC-2015- AdG Proposal No.694160). The authors also thanks to Spanish MINECO (CSO2010-11384- E, MAT2013-43299- R, MAT2015-64831- R, MAT2016-75611- R AEI/FEDER, E). The authors wish to thank the ICTS Centro Nacional de Microscopia Electrónica (Spain), CAI X-ray Diffraction, CAI NMR, CAI Flow Cytometry and Fluorescence Microscopy of the Universidad Complutense de Madrid (UCM, Spain) for the assistance.

References

[1] Campoccia D., Montanaro L., Arciola CR., The significance of infection related to orthopedic devices and issues of antibiotic resistance, Biomaterials, 2006, 27, 2331-2339.

[2] Lew D.P., Waldvogel F.A., Osteomyelitis, Lancet, 364 (2004) 369-379.

[3] Vila J., Soriano A., Mensa J., Molecular basis of microbial adherence to prosthetic materials. Role of biofilms in prosthesis-associated infection, Enferm. Infecc. Microbiol. Clin., 26, 2008, 48-54.

[4] Arciola C.R., Campoccia D., Speziale P., Montanaro L., Costerton J.W., Biofilm formation in Staphylococcus implant infections. A review of molecular mechanisms and implications for biofilm-resistant materials, Biomaterials, 33, 2012, 5967-5982.

[5] Götz F., Staphylococcus and biofilms, Mol. Microbiol., 43, 2002, 1367-1378.

[6] Harris L., Foster S.J., Richards R.G., An introduction to *Staphylococcus aureus*, and techniques for identifying and quantifying *S. aureus* adhesins in relation to adhesion to biomaterials: review, Eur. Cell Mater., 2002, 4, 39-60.

[7] Haidar R., Der Boghossian A., Atiyeh B., Duration of post-surgical antibiotics in chronic osteomyelitis: empiric or evidence-based?, Int. J. Infect. Dis., 14, 2010, 752-758.

[8] Huh A.J., Kwon Y.J., "Nanoantibiotics": A new paradigm for treating infectious diseases using nanomaterials in the antibiotics resistant era, J. Control. Release, 2012, 156, 128-145.

[9] Dvir T., Timko B.P., Kohane D.S., Langer R., Nanotechnological strategies forengineering complex tissues, Nat. Nanotechnol., 6, 2011, 13-22.

[10] Vallet-Regí M., Balas F., Arcos D., Mesoporous materials for drug delivery, Angew. Chem. Int. Ed., 2007, 46, 7548-7558.

[11] Baeza A., Colilla M., Vallet-Regi M., Advances in mesoporous silica nanoparticles for targeted stimuli-responsive drug delivery, Expert Opin. Drug Deliv., 2015, 12, 319-337.

[12] Wang Y., Zhao Q., Han N., Bai L., Li J., Liu L., Che E., Hu L., Zhang Q., Jiang T., Wang S., Mesoporous silica nanoparticles in drug delivery and biomedical applications, Nanomedicine, 2015, 11, 313-327.

[13] Martínez-Carmona M., Lozano D., Colilla M., Vallet-Regí M., Selective topotecan delivery to cancer cells by targeted pH-sensitive mesoporous silica nanoparticles, RSC Adv., 6, 2016, 50923-50932.

[14] Lei Q., Qiu W.-X., Hu J.-J., Cao P.-X., Zhu C.-H., Cheng H., Zhang X.-Z., Multifunctional mesoporous silica nanoparticles with thermal-responsive gatekeeper for NIR light-triggered chemo/photothermal-therapy, Small, 12, 2016, 4286-4298.

[15] Li X., Zhao W., Liu X., Chen K., Zhu S., Shi P., Chen Y., Shi J., Mesoporous manganese silicate coated silica nanoparticles as multi-stimuli-responsive T1-MRI contrast agents and drug delivery carriers, Acta Biomater., 30, 2016, 378-387.

[16] Castillo R.R., Colilla M., Vallet-Regí M., Advances in mesoporous silica-based nanocarriers for co-delivery and combination therapy against cancer, Expert Opin. Drug Deliv., 14, 2017, 229-243.

[17] Martínez-Carmona M., Lozano D., Baeza A., Colilla M., Vallet-Regí M., A novel visible light responsive nanosystem for cancer treatment, Nanoscale, 9, 2017, 15967-15973.

[18] Zhao S., Xu M., Cao C., Yu Q., Zhou Y., Liu J., A redox-responsive strategy using mesoporous silica nanoparticles for co-delivery of siRNA and doxorubicin, J. Mater. Chem. B, 5, 2017, 6908-6919.

[19] Chen X., Sun H., Hu J., Han X., Liu H., Hu Y., Transferrin gated mesoporous silica nanoparticles for redox-responsive and targeted drug delivery, Colloids Surf. B Biointerfaces, 152, 2017, 77-84.

[20] Vallet-Regí M., Rámila A., del Real R.P., Pérez-Pariente J., A new property of MCM-41: Drug delivery system, Chem. Mater., 13, 2001, 308-311.

[21] Lu J., Liong M., Li Z., Zink J.I., Tamanoi F., Biocompatibility, biodistribution, and drug-delivery efficiency of mesoporous silica nanoparticles for cancer therapy in animals, Small, 16, 2010, 1794-1805.

[22] Tang F.Q., Li L.L., Chen D., Mesoporous silica nanoparticles: synthesis, biocompatibility and drug delivery, Adv. Mater., 24, 2012, 1504-1534.

[23] Fu C., Liu T., Li L., Liu H., Chen D., Tang F, The absorption, distribution, excretion and toxicity of mesoporous silica nanoparticles in mice following different exposure routes, Biomaterials, 34, 2013, 2565-2575.

[24] Lin Y.-S., Abadeer N., Haynes C.L., Stability of small mesoporous silica nanoparticles in biological media, Chem. Commun., 47, 2011, 532-534.

[25] Paris J.L., Colilla M., Izquierdo-Barba I., Manzano M., Vallet-Regí M., Tuning mesoporous silica dissolution in physiological environments: A review, J. Mater. Sci. 52, 2017, 8761-8771.

[26] Rimmelé T., Boselli E, Breilh D., Djabarouti S., Bel J.C., Guyot R., Saux M.C., Allaouchiche B., Diffusion of levofloxacin into bone and synovial tissues, J Antimicrob. Chemother. 53, 2004, 533-535.

[27] Grün M., Lauer I., Unger K.K., The synthesis of micrometer- and submicrometer-size spheres of ordered mesoporous oxide MCM-41, Adv. Mater., 9, 1997, 254-257.

[28] Nieto A., Balas F., Colilla M., Manzano M., Vallet-Regí M., Functionalization degree of SBA-15 as key factor to modulate sodium alendronate dosage, Microporous Mesoporous Mater., 116, 2008, 4-13.

[29] De Juan F., Ruiz-Hitzky E., Selective functionalization of mesoporous silica, Adv. Mater., 12, 2000, 430-432.

[30] Zhuravlev L.T., The surface chemistry of amorphous silica. Zhuravlev model, Colloid Surf. A., 173, 2000, 1-38.

[31] Brunauer S., Emmett P.H., Teller E., Adsorption of gases in multimolecular layers, J. Am. Chem. Soc., 60, 1938, 309-319.

[32] Cicuéndez M., Izquierdo-Barba I., Portolés I., Vallet-Regí M., Biocompatibility and levofloxacin delivery of mesoporous materials, Eur. J. Pharm. Biopharm., 84, 2013, 115-124.

[33] Ratkowksy D.A., Handbook of Nonlinear Regression Models, M. Dekker, 1990, New York.

[34] García-Álvarez R., Izquierdo-Barba I., Vallet-Regí M., 3D scaffold with effective multidrug sequential release against bacteria biofilm, Acta Biomaterialia 49, 2016, 113-126.